RSC Advances

PAPER

View Article Online
View Journal | View Issue



Cite this: *RSC Adv.*, 2020, **10**, 26646

# Friction and mechanical properties of amino-treated graphene-filled epoxy composites: modification conditions and filler content

Tianjiao Bao,[ab] Zhiyong Wang,[b] Yan Zhao,[*a] Yan Wang[b] and Xiaosu Yi[b]

It remains a challenge for graphene to reach its full potential as a lubricant and wear-resistant material in thermosetting resin composites. In this study, the mechanical properties and friction properties of amino-treated graphene-filled epoxy composites, which were influenced by the conditions for the modification of graphene and filler content, were investigated. The mechanical properties were measured by tensile examination and the tribological properties were determined using a ball-on-disk tribometer. The results showed that the composite filled with amino-treated graphene for a short reaction time exhibited the best tribological behavior, where the friction coefficient was 57.9% lower than that of the pure resin and the wear rate was 92.2% less than that of the neat resin. Simultaneously, this amino-treated graphene also resulted in enhanced mechanical properties and $T_g$ in the nanocomposite, implying its good crosslinking network and strong interface strength. The wear track analysis demonstrated that the excellent wear resistance was induced by its improved toughness, which restrained the crack propagation of fatigue wear and decreased the size of debris, promoting the formation of a transfer film, and thus protecting the contact surface. The tribological properties also varied with the concentration of the nanofiller, which showed the best performance at 0.2 wt%. Through the optimization of the modification conditions and concentration, this work highlights a promising strategy for the application of graphene-related materials in the field of tribology.

Received 12th May 2020
Accepted 18th June 2020

DOI: 10.1039/d0ra04237d

rsc.li/rsc-advances



## 1. Introduction

Graphene, which is well-known for its excellent properties such as high mechanical properties and atomic-scale lubricant properties,[1–3] has been recognized as an important promising lubricant.[4–6] For practical applications, it is promising as a lubricant and wear-resistant material to fabricate graphene-based composites and coatings.[7,8] Significant research on the tribological properties and mechanism of graphene-filled thermoplastic composites has been reported. However, the tribological mechanism is different and more complicated for thermosetting composites since the groups on nanoplatelets affect the curing reaction and construction of the crosslinking network.[9,10] Epoxy as a thermosetting resin has been commonly applied in lubricating coatings owing to its strong adhesion and physical properties. However, epoxy resins are inherently brittle and have a poor antiwear performance, which limit their applications. Thus, various nano-additives have been used to enhance their physical properties and antiwear properties.[11–13] Graphene oxide (GO) is mostly used[14,15] as a lubricant since it is easy to obtain *via* chemical oxidization and exfoliation of graphite.[16–19] Nevertheless, the enhancement in tribological properties is far below expectation, even exhibiting a decrease in lubricating properties.[20–22] One possible reason for this may be that GO tends to decompose under the processing heat or friction heat due to its lattice defects and numerous oxygen-containing groups.[23] Another explanation is that the strong polarity of GO makes it difficult to disperse in nonaqueous solvents and polymers. Plenty of research also showed that GO affects the curing reaction and decreases the glass transition temperature of polymers,[24,25] resulting in poor mechanical properties. Thus, it seems that GO is not the ideal graphene derivative structure as a lubricant for epoxy. Plenty of methods have been reported for the modification of graphene, which improve the interface interaction and enhance the mechanical properties of epoxy.[26–29] For instance, Wan YJ *et al.*[28] reported the enhanced glass transition temperature and mechanical properties of epoxy composites filled with silane-modified GO sheets. Xu *et al.*[29] prepared activated thermally exfoliated graphene (a-TEG) nanosheets to improve the interface between the nanofiller and epoxy. The tensile and flexural strength of a-TEG/epoxy increased by 20% and 50% compared to that of TEG/epoxy, respectively. The tribological performance is a comprehensive property, which not only relies on the mechanical properties, but also influenced by the thermal properties and lubricity of nanofillers. The intrinsic structure of graphene is

[a]*Department of Materials Science and Engineering, Beihang University, Beijing, 100191, China. E-mail: jennyzhaoyan@buaa.edu.com*
[b]*Beijing Institute of Aeronautical Materials, Beijing, 100095, China*

beneficial for the lubricating property and heat resistance, which may have effect on the tribological properties. Thus, reduction treatment needs to be introduced to recover the ordered structure of graphene. Long-chain aliphatic amine (octadecylamine, ODA) treatment for GO is a one-step procedure to realize surface functionalization and reduction of graphene oxide simultaneously,[30] and the resulting ODA-modified graphene was reported to be well-dispersed in non-aqueous solvents. Therefore, amino-treated graphene (rGO) possesses higher thermostability than GO, and simultaneously, it can be compatible with resins and interact with epoxy due to its amino groups. For amino treatment,[31–34] the morphology and chemical structure (reduction degree and the active groups) of modified GO change with the reaction conditions (reaction temperature and reaction time), which influences the nanoscale tribological properties of graphene, curing reaction, and interface connection, thus affecting the final properties. Consequently, inspired by these considerations, the effect of the chemical structure of graphene on the mechanical properties and tribological performance of nanocomposites should be investigated. This is important for practical application since it would guide researchers on how to control the amine treatment reaction for the optimum results.

In our previous studies,[35] the morphology, structure and dispersity of rGO under different reaction conditions were investigated, and we found that the morphology and structure of the as-prepared rGO changed with the reaction time. Intense conditions (high temperature and long time) were selected in our previous work on amino modification, for instance, 80 °C and 24 h, respectively.[36] These reaction conditions were used for the amino modification reaction of carbon nanotubes,[37] in which amine reacted with the carboxyl group on the acidic carbon nanotubes. However, the reaction of amine with the epoxide group on GO was totally different, which could occur instantaneously. Therefore, it is doubtful if it is necessary to prepare modified GO using such a long reaction time. In this work, graphene oxide was treated with ODA for a long and short time to obtain modified GO with two typical structures. Composites were prepared by incorporating three types of graphene nanosheets into the epoxy matrix to compare their tribological performance. It was found that GO treated with for a short time was beneficial for the tribological performance of the epoxy-based composites. Furthermore, we investigated the principle factors and mechanism responsible for the tribological performance and attempted to determine the relationship between tribological performance and structure/content of graphene.

## 2. Experimental

### 2.1. Materials

Graphene oxide (GO) was supplied by Beijing Institute of Aeronautical materials, which was synthesized *via* a modified Hummer's method.[27] AR grade octadecylamine (ODA), ethanol, and tetrahydrofuran (THF) were purchased from Sinopharm Chemical Reagent Co., Ltd. Epoxy resin (E-51) was provided by China National Bluestar (Group) Co. Ltd. O,O-bis(2-aminopropyl) polypropylene glycol D230, which was used as the curing agent for epoxy, was a product of Huntsman Company.

### 2.2. Preparation of amino-treated graphene oxide

Before treatment, 0.1 g of GO was added to a flask with ethanol (200 mL), and the suspension was sonicated for 30 min. Subsequently, 0.5 g of ODA well-dispersed in ethanol (3 mL) was poured into the flask, which was refluxed with magnetic stirring at 80 °C for 0.5 h and 5 h (recorded as rGO-0.5 and rGO-5, respectively). The modified graphene oxide (rGO) was washed 5 times with hot ethanol and collected by vacuum filtration. The filtered material was finally dried under vacuum at 70 °C for 3 h.

### 2.3. Graphene-based composite

In a typical preparation process, a certain amount of filler and epoxy resin were added to a beaker with THF and sonicated for 30 min, and then the organic solvent was removed with a rotary evaporator at 60 °C and −0.1 MPa for 30 min. The prepared mixture was cooled in ice water for 5 min. Then the cured agent was filled with a ratio of 31 : 100 D-230 to epoxy and mechanically stirred for 20 min. The mixture was left to stand at 45 °C for 20 min to remove air bubbles. Subsequently, the mixture was poured into an open mould and cured at 50 °C for 3 h, then 100 °C for 2 h. After curing, the specimens were kept in a furnace to room temperature. To explore the variation in mechanical properties and tribological properties with the structure of graphene, neat epoxy resin and epoxy composites with weight fractions of 0.2 wt% of GO, rGO-0.5 and rGO-5h were prepared. Meanwhile, epoxy composites with 0.1 wt%, 0.2 wt%, 0.3 wt%, and 0.4 wt% of rGO-0.5 were prepared to study the effect of the concentration of rGO-0.5.

### 2.4 Characterization

The morphology of GO and rGO were analysed *via* atomic force microscopy (AFM) using a Multimode 8 instrument (Bruker, Germany) in a scan assist mode. To prepare the AFM samples, a THF suspension of GO/rGO was dropped onto freshly cleaved mica, and then dried in air. XPS measurements were performed using an Escalab 250XI (ThermoFisher Scientific, America), with a power of 150 W. X–ray diffraction (XRD) patterns were measured using a D8 Advance diffractometer (Bruker, Germany) with a Cu K$\alpha$ source ($\lambda$ = 0.1546 nm). TGA of GO/rGOs was carried out from ambient temperature to 800 °C with an SDTQ600 thermobalance (TA Instruments, America) at a heating rate of 10 °C min$^{-1}$ in air. The dispersity and morphology of GO and rGO in THF were observed *via* optical microscopy using a BX51M microscope. The optical micrograph samples were prepared in the same way on glass slides as the AFM samples. A GB/T2568 was used to determine the tensile strength, modulus, and elongation at break. The loading speed was 3 mm min$^{-1}$, and 5 samples of each composite were tested. Differential scanning calorimetry (DSC) with a Q200 (TA, America) was performed under a nitrogen atmosphere from room temperature to 150 °C at 10 °C min$^{-1}$. The data was recorded after erasing the previous thermal history, and the glass transition

temperature ($T_g$) was determined from the midpoint of the transition steps. The hardness was determined using a G200 nano-indenter (Agilent, America), controlling the pressed depth at 500 nm. The resulting values were the average of ten measurements. The tribological performances were investigated using a tribometer (UMT-3, CETR, USA) in the ball-on-disk reciprocating mode. The upper ball was a GCr15 steel ball (diameter of 12.7 mm and surface hardness of 63(HRC)). The test conditions were set as a load of 5 N at a sliding speed of 0.1 m $s^{-1}$, with a reciprocating radius of 5 mm, and a testing time of 60 min. Wear loss was measured using a three-dimensional white-light interferometer (Nexview, Zygo, America). The tribological test was repeated 3 times for each point, and the mean of three different test results was calculated as the average coefficient of friction (COF) and wear rate. Scanning electron microscopy (SEM) images of the wear track and fracture morphology were taken using a Nova NanoSEM microscope (FEI, America) after coating with a thin layer of gold. The wear track was also observed using a BX51M microscope (Olympus, Japan).

## 3. Results and discussion

### 3.1 Characterization of amino-treated graphene

The variation in the functional groups on the graphene sheet with different reaction time observed by FTIR spectroscopy was reported in our previous work.[35] The removal of numerous oxygenic groups, the characteristic peak of the linear connection in methyl groups at 720 $cm^{-1}$, and the characteristic peaks of the amino group demonstrated the successful chemical reduction and surface grafting of the ODA chains.

The AFM images and their height profiles showed the dimension, morphology and thickness of three different graphene sheets. Due to the wrinkles in the GO sheets, a thickness in the range of 0.5 nm and 1 nm was observed (Fig. 1a), which is consistent with that reported for single-layer GO.[38] The AFM images also revealed that the dimensions of the GO sheets were in the range of 10–30 μm, and numerous defects on the GO sheets were also observed. The dimensions of rGOs decreased drastically to a few hundred nanometers upon amine treatment, which was induced by the elimination of most of the functional groups. It also observed that the thickness of the rGO-0.5 sheet increased to 1 nm (Fig. 1b) due to the long chains attached on the surface of GO. However, the thickness of the rGO-5 sheet was up to 2 nm (Fig. 1c), which was caused by the accumulation of the rGO-5 platelets. As confirmed by the chemical analysis, the oxygenic groups such as hydroxyl and epoxide groups on GO were affected greatly under the condition of long reaction time, leading to a strong tendency to restack in the rGO-5 nanosheets.

The XRD patterns (Fig. 2) confirmed the chemical graft and reduction of rGOs upon amine modification. In the diffraction pattern of GO, a diffraction peak was observed at around $2\theta = 10.2^{\circ}$. According to Bragg's law, the calculated value of $d$ was determined to be 8.67 Å, which is in accordance with the

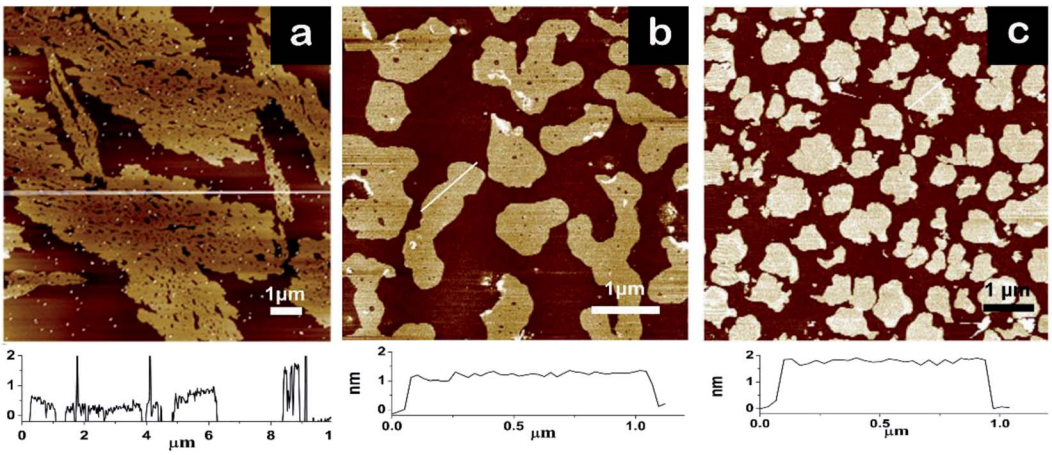


Fig. 1 AFM images of GO/rGOs. (a) GO. (b) rGO-0.5 and (c) rGO-5.

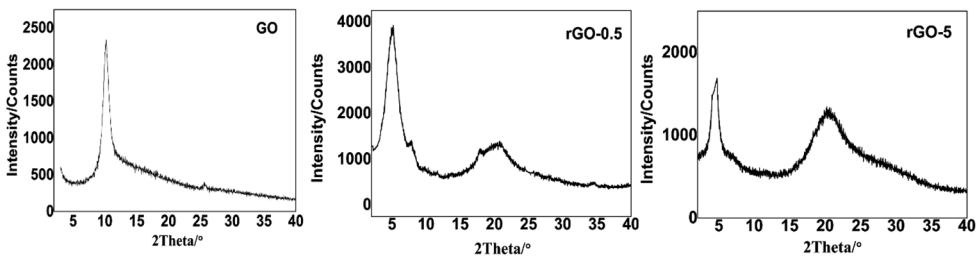


Fig. 2 XRD patterns of GO/rGOs (a) GO, (b) rGO-0.5, and (c) rGO-5.

 

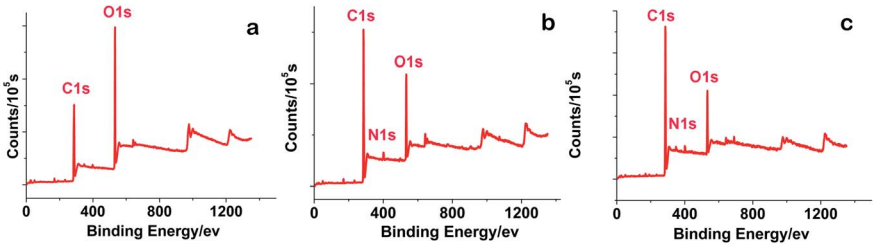


Fig. 3 XPS spectra of GO/rGOs (a) GO, (b) rGO-0.5, and (c) rGO-5.

Table 1 Atomic ratio of GO/rGOs from XPS result

| No. | Name | C 1s atomic% | N 1s atomic% | O 1s atomic% |
|---|---|---|---|---|
| 1 | GO | 65.52 | 0 | 34.48 |
| 2 | rGO-0.5 | 78.82 | 3.06 | 18.12 |
| 3 | rGO-5 | 82.48 | 2.96 | 14.56 |

reported value.[39] In contrast, there were two diffraction peaks in the XRD patterns of rGO-0.5 and rGO-5, which were located at $2\theta = 4.9^\circ$ and $2\theta = 20.8^\circ$, respectively. The XRD patterns of rGOs indicated that the graphene sheets became a mixture of two types of nanoparticles upon modification. One type of graphene sheet was grafted by long alkyl chains, and the distance between layers increased to 18 Å ($2\theta = 4.9^\circ$). Meanwhile, the other type of graphene sheet was restacked (the value of $d$ is around 4.25 Å, $2\theta = 20.8^\circ$) due to the elimination of the oxygenic group, which was induced by the reduction effect.[40] It was obvious that the well exfoliated graphene was dominant in rGO-0.5 according to the intensity of the different peaks, while the restacked type was dominant in rGO-5, which provided evidence that rGO-5 restored the aromatic structure of graphene to a greater extent.

XPS (Fig. 3) was performed to further investigate the chemical structure of GO/rGO. The peaks at 284.7 eV, 401.1 eV and 532.2 eV correspond to C, N and O, respectively.[41] The atomic ratio of C, O and N is presented in Table 1. The results show that the ratio of C : O was about 2 : 1 in the GO spectrum, while that of rGO-0.5 and rGO-5 was about 4 : 1 and 5 : 1, respectively. Thus, these results verify the reduction reaction between GO and ODA, and that the reduction degree increased with a longer reaction time. In summary, the oxygenic groups on the rGO-0.5 sheet were reduced compared with GO, while that on the rGO-5 platelets was mostly removed. In the XPS spectrum of rGOs, signals at 399.5 eV corresponding to C–N appeared,[42] which were not observed in the XPS of GO, revealing that the ODA chains were attached to the graphene sheets.

The dispersion of the graphene derivatives in solvent can be reflected by their dispersion state in epoxy indirectly, which was characterized *via* optical microscopy. According to the experimental section, the samples were prepared by dropping a THF suspension of GO/rGO onto glass slides, and then drying naturally. As shown in Fig. 4a, the GO nanosheets aggregated, which mostly existed in the form of wrinkled paper in THF. When epoxy was incorporated in the system, the wrinkled morphology of GO reduced its real contact area with the resin, and air and related defects were easily wrapped in the composite. Then, according to Fig. 4b, the rGO-0.5 nanosheets were dispersed uniformly, and the nanosheets exhibited an unfolded flake-like shape, which provided a large specific surface area to interact with the epoxy resin. In addition, the chemical analysis demonstrated rGO-0.5 possessed both amino chains and residual oxygenic group, which could interact well with epoxy. Furthermore, rGO-0.5 could also be dispersed well in THF, as shown in Fig. 4c. However, due to the high degree of reduction of rGO-5 based on the XPS analysis, it was prone to restacking, and thus the pieces were darker.

TGA analysis of GO/rGO was performed to study the thermostability of the different graphene samples. As shown in Fig. 5, the weight loss of GO occurred below 100 °C, and reached 10% at 150 °C. This result is similar to that observed in previous research.[43] In contrast, the ODA-treated graphene oxide showed enhanced thermostability, implying that the removal of the thermally labile oxygen-containing groups improved the thermal stability of the amino-treated GO. For example, negligible weight loss of rGOs was achieved below 100 °C. This

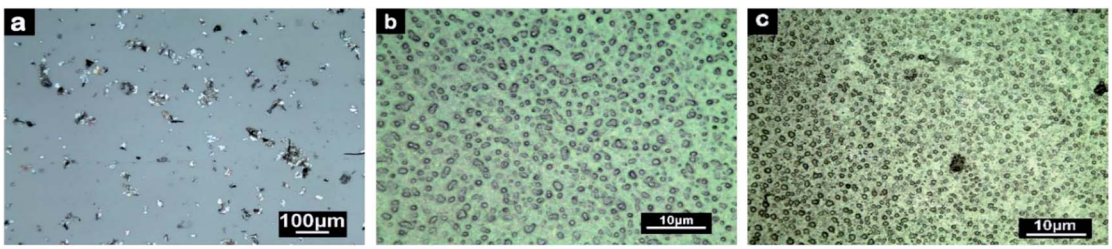


Fig. 4 Optical micrographs of GO (a), rGO-0.5 (b) and rGO-5 (c) in THF suspension.

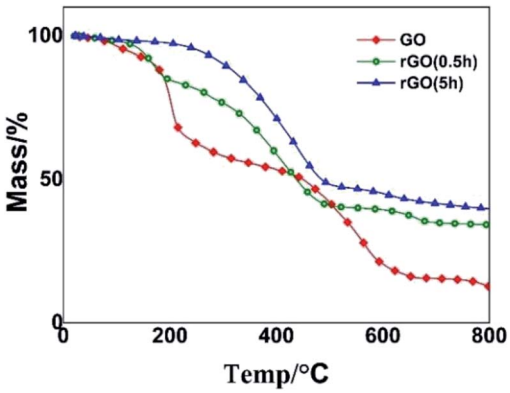


Fig. 5 TGA curves of graphene with three different structures.

remarkably enhanced thermostability is essential for the performance of thermoset composites due to the inevitable heat during their preparation and the service process.

The characterization of GO/rGO depicted three different structures and morphologies in the graphene derivatives, and their models are displayed in Scheme 1. For GO (Scheme 1a), it possessed large dimensions, plenty of oxygen-containing groups, and many wrinkles in its nanosheets. However, the structure of rGO-0.5 (Scheme 1b) changed remarkably, which showed smaller dimensions, long amino chains and an increase in the distance between the nanosheets. Additionally, rGO-5 exhibited a chemical structure close to that of ideal graphene (Scheme 1c), but most of its nanosheets were restacked. The structures of rGO-0.5 and rGO-5 are both beneficial for the tribological performance. For instance, rGO-0.5 containing more chemical groups can interact well with epoxy. The recovery of the graphitic structure and increase in the number of layers of rGO-5 contribute to its lubricating properties.[3,44] Consequently, to determine which factor will be dominant in the tribological performance of the epoxy composites, the effect of the structure and morphology of the nanoplatelets on the tribological properties of the composites was investigated.

### 3.2 The effect of modification conditions on the properties of the composites

The mechanical properties of the nanocomposites with different fillers obtained by tensile examination at room temperature are summarized in Table 2. The nanocomposites with the fillers exhibited enhanced tensile strength and Young's modulus. The enhancement in mechanical properties by adding rGO-0.5 nanosheets was found to be the most obvious, that is, the strength was enhanced by 14%, and the modulus increased by 25%. A more significant improvement was exhibited in toughness, that is, the elongation at break increased two-fold compared with that of the pure resin. The relatively large improvement in the properties of the rGO-0.5 composite is attributed to the effective load transfer from the epoxy matrix to the nanosheets since the amino groups greatly improved their dispersion and interfacial adhesion with the matrix. The GO composite exhibited a lower modulus and strength, and almost no enhanced ductility was achieved. The rGO-5 composite also exhibited less enhancement compared with the rGO-0.5 composite.

Table 2 Mechanical properties of pure resin and composites with GO/rGOs

| No. | Sample | Modulus (GPa) | Strength (MPa) | Elongation (%) |
|---|---|---|---|---|
| 1 | Epoxy | 2.55 ± 0.17 | 65.2 ± 1.8 | 1.0 ± 0.3 |
| 2 | GO/EP | 3 ± 0.12 | 70.8 ± 1.6 | 1.2 ± 0.2 |
| 3 | rGO-0.5/EP | 3.2 ± 0.10 | 74.2 ± 2.1 | 3.4 ± 0.2 |
| 4 | rGO-5/EP | 2.94 ± 0.12 | 70.4 ± 1.2 | 2.0 ± 0.4 |

The fracture morphology of the composites is shown in Fig. 6, which displays the influence of the nanofillers on the fracture process. In Fig. 6a, the fracture morphology of the neat epoxy appears to be the typical brittle fracture, which is mirror-like fracture face, demonstrating the rapid crack propagation. The brittleness of the epoxy is attributed to its high cross-link density, which led to the poor absorption of energy during fracture. The fracture surface was still smooth with plenty of microcracks when GO was added, implying that the brittleness of the epoxy did not weaken. The rapid crack propagation in the GO/epoxy composites resulted from microcracks (shown in Fig. 6b), which were introduced by the wrinkled GO and decomposition of GO by heat. These defects eventually became crack sources and accelerated crack growth. Unlike the smooth fracture surface of the pure resin, the coarse and multiplane feature of rGO-0.5/epoxy fracture surface in Fig. 6c illustrate that the propagation of cracks was restrained and decelerated significantly by the amino-functionalized rGO-0.5 nanosheets. The well-impregnated graphene sheets induced the deflection of propagating crack fronts and generated plenty of new fracture surfaces, which exhausted more fracture energy.[51,52] The rGO-5 nanosheets could also hinder the crack propagation since their fracture surface also showed a river-like pattern with numerous branches (Fig. 6d). However, the fracture surface of rGO-5 was smoother due to its weak interface interaction with

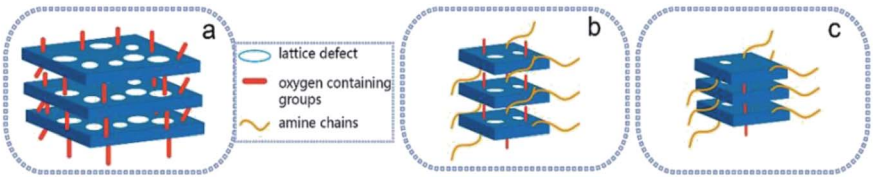


Scheme 1 Structural models of the different types of graphene (a) GO, (b) rGO-0.5 and (c) rGO-5.

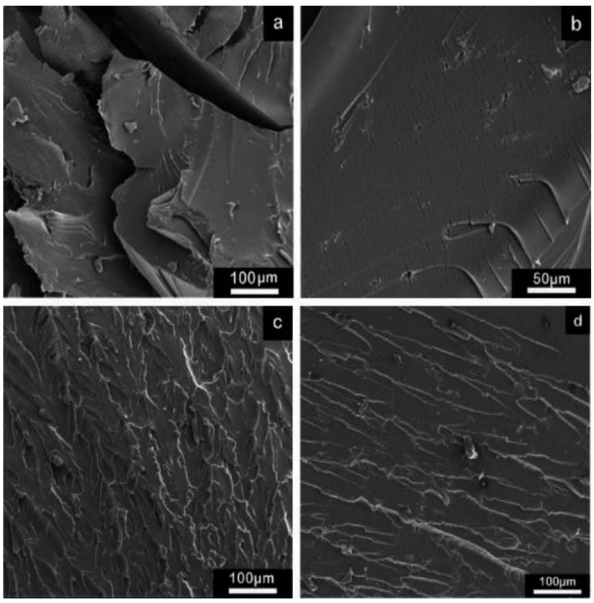


Fig. 6 Fracture morphology of the pure resin and composites with GO/rGOs by SEM. (a) Pristine resin, (b) GO composite, (c) rGO-0.5 composite and (d) rGO-5 composite.

the matrix compared with the rGO-0.5 composites, as inferred by the few functionalized group structures of rGO-5.

The glass transformation temperature ($T_g$), which is related to the movement of the chain segments, was further examined to reflect the network and interface of the composites.[49] The $T_g$ of the composites was tested by DSC (Table 3). As shown in Table 3, the $T_g$ of rGO-0.5/epoxy increased by 6.4 °C compared with that of the pure resin, while the GO/epoxy composite and rGO-5/epoxy demonstrated a slightly lower $T_g$ compared with the pure resin. The reduction of the $T_g$ of GO/epoxy[23,50] was previously attributed to the consumption of the curing agent by GO, which lowered the crosslinking density. Also, the large sheet of GO and wrinkles physically hinder the approach of the curing agent to the epoxy resin. In the case of rGO-0.5, as a contrast, the oxygen- and amine-containing groups could interact with the curing agent and epoxy resin respectively, which acted as a bridge in the network of the composites, and therefore restricted the mobility of the polymer chains. However, owning to the inactive surface and restacking of the rGO-5 sheets, the interface of rGO-5 and epoxy became poor. Therefore, the low $T_g$ of the rGO-5/epoxy composite can be attributed to the poor interface between rGO-5 and epoxy, which provided more space for the movement of the chain segments.

The surface hardness, as an important factor, can affect the antiwear properties. Fig. 7 shows the microhardness of the

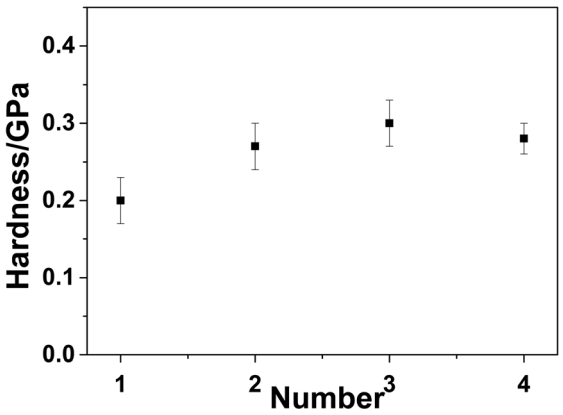


Fig. 7 Surface hardness of the pure resin and composites with GO/rGOs tested by nanoindentor (1#. pure resin; 2#. GO composite; 3#. rGO-0.5 composite; 4#. And rGO-5 composite).

neat epoxy and composites, which was determined using a nanoindenter. As shown in Fig. 7, the surface hardness of the composite was higher than that of the pure resin, especially the hardness of the rGO-0.5/epoxy increased by 24% compared with the pure resin. The enhancement mechanism of the hardness of the composite by adding nanofiller was well investigated, indicating that the high strength the nanofiller shared part of stress and a good interface is necessary for stress transfer. The mechanical improvement of GO/epoxy and rGO-5/epoxy was much less than rGO-0.5/epoxy, which was associated with the distribution of nano fillers and interface of composites.[48]

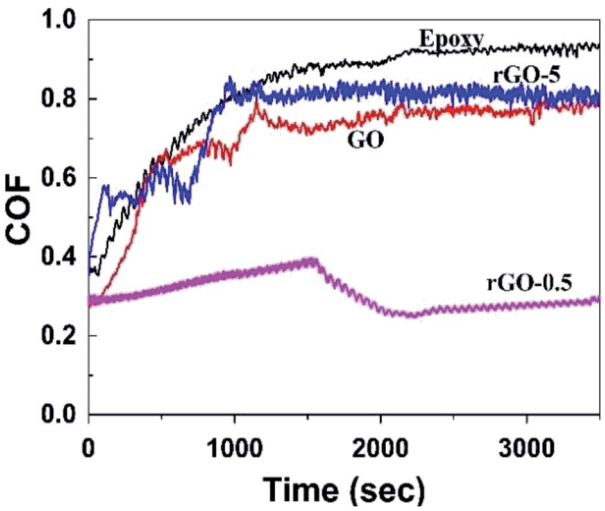


Fig. 8 COF curves of pure resin and composites with GO/rGOs.

Table 3 $T_g$ of the pure resin and composites with GO/rGOs

| No. | 1 | 2 | 3 | 4 |
|---|---|---|---|---|
| Name | Pure resin | GO composite | rGO-0.5 composite | rGO-5 composite |
| $T_g$/°C | 79.6 | 79 | 86 | 79.2 |

Table 4 Average COF of the pure resin and composites with GO/rGOs

| No. | 1 | 2 | 3 | 4 |
|---|---|---|---|---|
| Name | Pure resin | GO composite | rGO-0.5 composite | rGO-5 composite |
| ACOF | 0.76 ± 0.07 | 0.70 ± 0.06 | 0.32 ± 0.04 | 0.72 ± 0.03 |

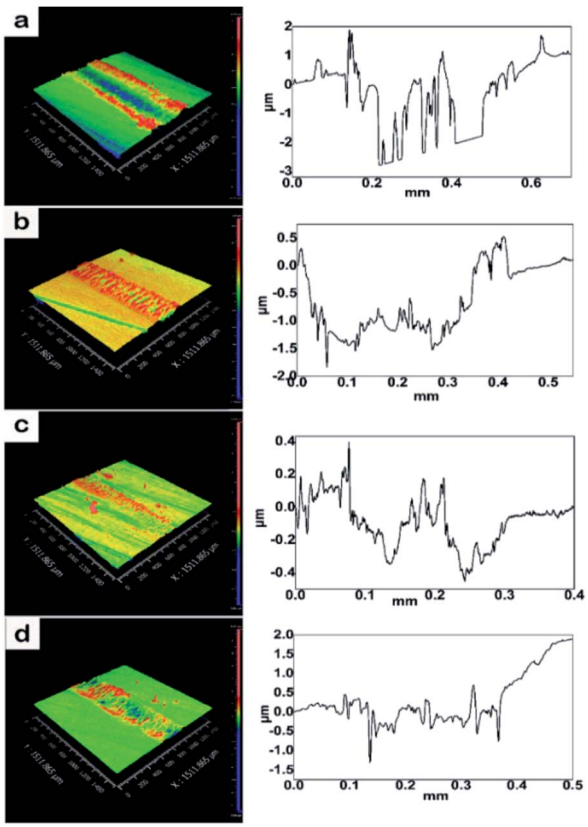


Fig. 9 Wear track of the pure resin and composites with GO/rGOs and their corresponding height profiles (a) pure resin, (b) GO composite, (c) rGO-0.5 composite, and (d) rGO-5 composite.

The COF and wear rate of the pristine epoxy, GO/epoxy, rGO-0.5/epoxy, and rGO-5/epoxy were investigated under a load of 5 N for 60 min. The variation in the friction coefficient is presented in Fig. 8. The COF curve exhibited the typical performance of resin-based composites,[45,46] that is, there were two characteristic stages, a running-in stage and steady stage. The average friction coefficients are summarized in Table 4, in which the average COF value of the neat epoxy was the highest (0.76). The friction coefficient decreased drastically after incorporating GO/rGOs into the epoxy resin. In particular, the average COF value of rGO-0.5/epoxy was the lowest (0.32), which was lower than that of the pure resin by 57.9%. The decrease in the average COF of GO/epoxy and rGO-5/epoxy was not as obvious compared with rGO-0.5.

The wear track of the GO/rGO composites and their corresponding height profiles at room temperature are shown in Fig. 9. The volume of the wear track was measured using a white light interferometer, and the wear rate ($K$, $mm^3\ N^{-1}\ m^{-1}$) of the specimen was calculated using the following equation:

$$K = \frac{\Delta V}{0.1Ft} \quad (1)$$

where $\Delta V$ is the wear volume ($mm^3$), $F$ demotes the applied load ($N$), and $t$ the experimental duration (s).

The reduction in the wear rate exhibited a similar trend as variation in the average COF (Table 5). The rGO-0.5 composite showed the best anti-wear properties, where the wear rate was reduced by 92.2% compared to that of the neat resin. Although previous work[8,14] showed the enhancement effect of graphene on wear resistance, a significant improvement in wear resistance (over 92%) by graphene nanosheets has rarely been reported.

The wear track of both the contact surfaces and wear debris provided information of the friction behavior and wear mechanism, which are presented in Fig. 10 and 11, respectively. The wear track of the neat epoxy exhibited serious fatigue wear, in which numerous deep cracks were observed (Fig. 10a and a-1). A high stress concentration promoted crack initiation and rapid propagation under reciprocating friction due to the low modulus and high brittleness of the neat epoxy, resulting in severe fatigue wear. In contrast, the SEM image of the rGO-0.5 composite showed a shallow and smooth wear track (Fig. 10c), with extremely tiny microcracks in the magnified image in Fig. 10c-1. Due to its structural feature, rGO-0.5 was well dispersed in the epoxy and could provide active groups to interact with the resin, which facilitated load transfer to the nanosheets and restrained crack propagation. Therefore, the

Table 5 Quantitative analysis of the wear track of the pure resin and GO/rGOs composites

| No. | Name | Wear volume ($mm^3$) | Wear rate ($mm^3\ N^{-1}\ m^{-1}$) |
|---|---|---|---|
| 1 | Purec resin | $(16.4 \pm 0.12) \times 10^{-3}$ | $(9.11 \pm 0.07) \times 10^{-6}$ |
| 2 | GO composite | $(6.9 \pm 0.15) \times 10^{-3}$ | $(3.82 \pm 0.08) \times 10^{-6}$ |
| 3 | rGO-0.5 composite | $(1.3 \pm 0.10) \times 10^{-3}$ | $(0.71 \pm 0.05) \times 10^{-6}$ |
| 4 | rGO-5 composite | $(3.6 \pm 0.16) \times 10^{-3}$ | $(2.01 \pm 0.09) \times 10^{-6}$ |

 

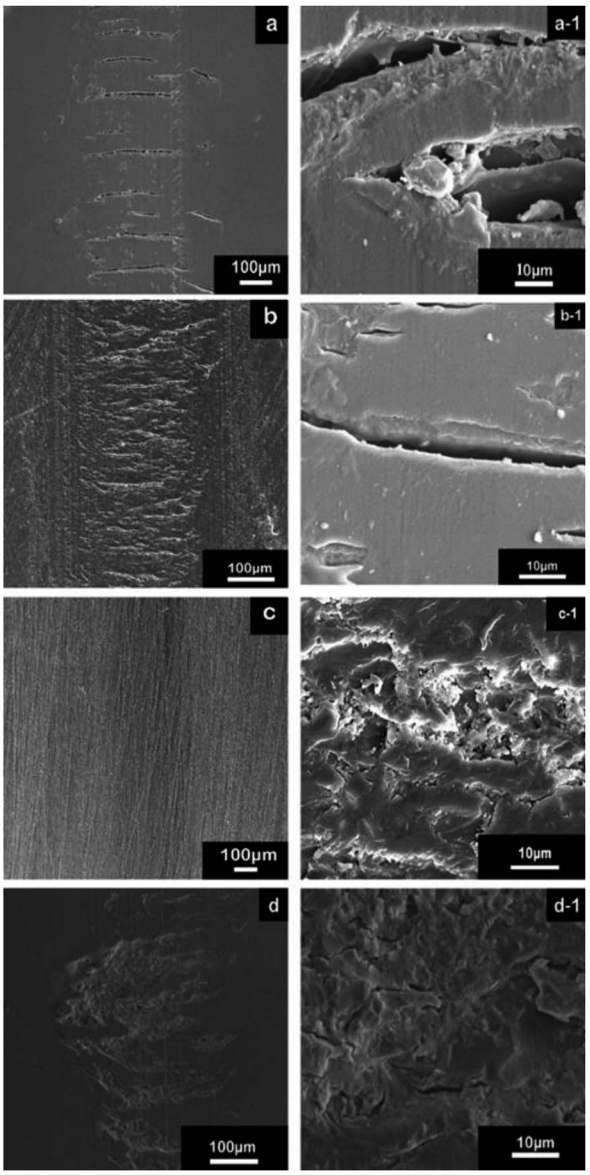


Fig. 10 SEM images of the wear surface of the pure resin and composites with GO/rGOs. (a) Pure resin and (a-1) partial magnification of (a). (b) GO composite and (b-1) partial magnification of (b). (c) rGO-0.5 composite and (c-1) partial magnification of c. (d) rGO-5 composite and (d-1) partial magnification of (d).

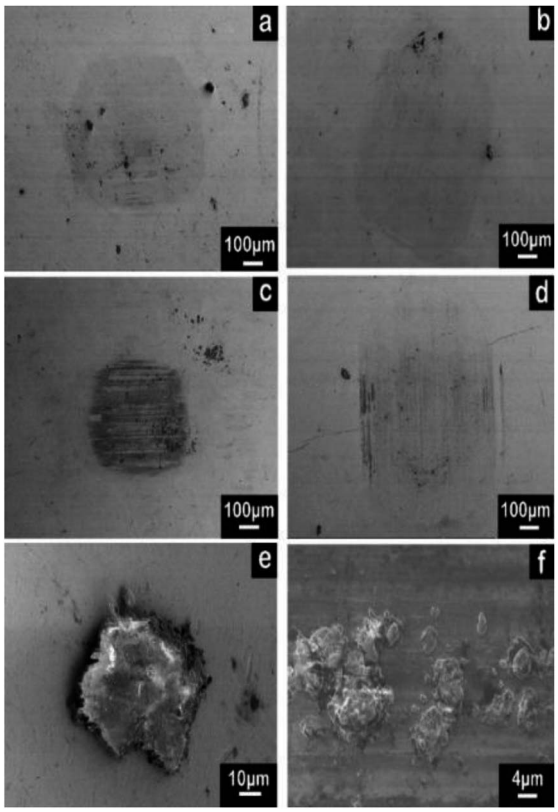


Fig. 11 SEM image of the wear scars on the contact steel ball with the different composites and the wear debris. (a) Epoxy, (b) GO composite, (c) rGO-0.5 composite, (d) rGO-5 composite, (e) debris from pure epoxy, and (f) debris from rGO-0.5 composite.

wear of the rGO-0.5 composite was transformed to mild fatigue wear. Furthermore, it was difficult for a large piece of resin to peel off from the wear surface because of the high dispersity and strong interface interaction. Consequently, the wear debris of the rGO-0.5/epoxy composite (Fig. 11f) was much smaller than that in the neat epoxy (Fig. 11e). The resultant small debris was easier to form a continuous transfer film, which further decreased the surface wear. Meanwhile, the increase in glass transition temperature and enhancement in thermal conductivity by adding rGO-0.5 allowed the nanocomposite to withstand a higher friction heat, which is another factor that enhances the wear resistance. In comparison, the cracks on the wear track of GO and the rGO-5 composite were much deeper than that of rGO-0.5/epoxy (Fig. 10b, b-1, d and d-1). In addition, the wear track of the rGO-5 composite showed deep grooves, indicating abrasive wear. According to their mechanical properties, the improvement in the toughness of the GO/epoxy composites was limited, and thus the fatigue crack could grow rapidly. In the case of rGO-5, it tended to restack due to the Van der Waals force between the nanosheets,[53] and the interface interaction in rGO-5/epoxy was much weaker due to the shortage of active groups. Although graphene with more layers has a lower friction coefficient, due to the lack of good dispersity and interfacial interaction, its intrinsic lubricating properties could not be activated. Even worse, the agglomerated nanoplatelets behaved as abrasive particles to increase the abrasive wear. Therefore, the ability to resist both deformation and crack growth was weakened in the GO-composite and rGO-5 composite. Consequently, they exhibited poor wear resistance compared to the rGO-0.5 composite.

In this work, both normal load and sliding velocity were constant. According to classical tribological theory,[47] the friction force depends on the definition of the product of the real contact area and shear strength. The real contact area is influenced by the extent of deformation and roughness of the contact surface. The rGO-0.5 composite exhibited both less deformation due to its high modulus and smooth contact surface, resulting in a smaller real contact area. According to the

SEM image of the wear scar contacting with the rGO-0.5 composite (Fig. 11c), a black transfer film was observed, which was more obvious and complete than that on the other samples. The transfer film could separate the contact surfaces, preventing them from direct contact. Therefore, the shear strength was reduced greatly by the lamellar and loose transfer film. Consequently, the COF of the rGO-0.5 composite was the lowest. In the case of the pure epoxy, GO composite and rGO-5 composite, their rough contact surface could not form a complete transfer film (Fig. 11a, b and d), leading to a higher COF, respectively. Thus, according to the above analysis, it can be concluded that the tribological properties of the epoxy-based nanocomposites are closely related to the distribution of nanofiller and their interface property. A uniform distribution of nanofiller results in small wear debris, which contributes to the formation of a continuous transfer film. The strong interface interaction can enhance the crack propagation resistance of the composites, which can restrict fatigue wear. The intrinsic lubricating properties of the nanoparticles can be activated only when they interact well with the matrix.

### 3.3 The effect of filler content on the properties of the composites

The concentration of fillers is another important factor influencing the tribological performance of the nanocomposites. The variation in the friction coefficients of the rGO-0.5/epoxy composites with the concentration of rGO-0.5 is shown in Fig. 12, and the average friction coefficient (COF) is presented in Table 6. The results demonstrate that the friction coefficient decreased with an increase in the concentration of rGO-0.5 initially, and then increased after the content exceeded the optimum value of 0.2 wt%.

The variation in wear (Fig. 13 and Table 7) showed the same trend as that of COF. Therefore, the composite containing 0.2 wt% filler also showed the best wear resistance performance. According to the analysis of friction and wear mechanism above, the friction and wear properties are closely related to the distribution of nanosheets and the interface properties.

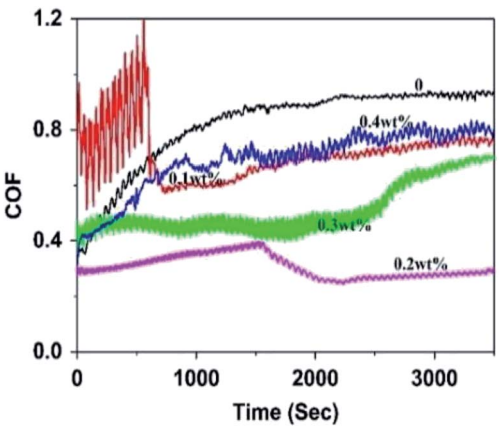


Fig. 12 The variation of friction coefficient of the rGO-0.5/epoxy composites with different filler content.

Table 6 Average friction coefficients of the rGO-0.5/epoxy composites with different filler contents

| No. | Content (wt%) | COF |
|---|---|---|
| 1 | 0 | 0.76 ± 0.07 |
| 2 | 0.1 | 0.69 ± 0.03 |
| 3 | 0.2 | 0.32 ± 0.04 |
| 4 | 0.3 | 0.51 ± 0.03 |
| 5 | 0.4 | 0.62 ± 0.04 |

Neither a low filler content nor high filler content had a positive effect on the distribution and the interface interaction. When the filler content was low, the filler had a limited improvement effect on the resin, which also maintained poor lubricating properties. Besides, for the composite with a higher concentration, for instance 0.4 wt%, the nanofiller could not disperse well and was apt to agglomerate in the composite, which induced defects and abrasive particles, resulting in severe fatigue wear. Therefore, the composites with 0.1 wt% and 4 wt%

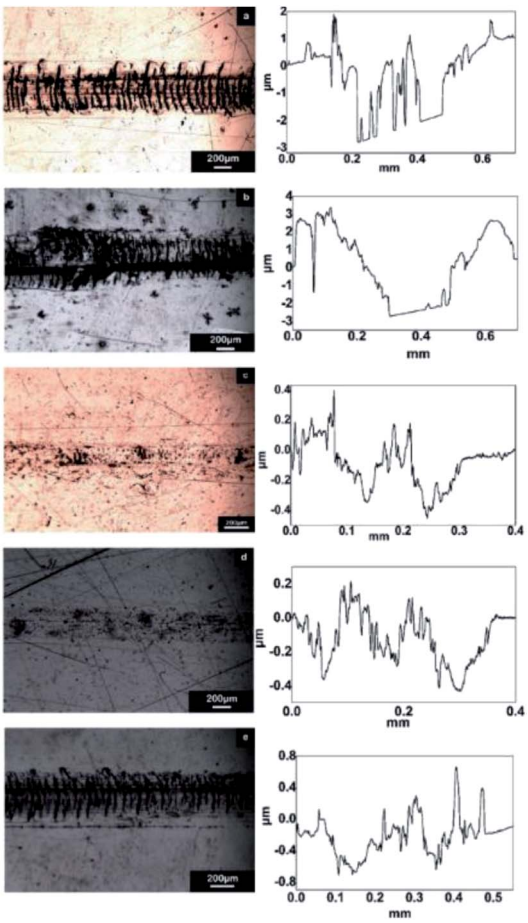


Fig. 13 Wear track of the rGO-0.5/epoxy composites with different filler contents and the corresponding height profiles. (a) Pure resin, (b) composite with 0.1 wt% rGO-0.5, (c) composite with 0.2 wt% rGO-0.5, (d) composite with 0.3 wt% rGO-0.5, and (e) composite with 0.4 wt% rGO-0.5.

Table 7 Quantitative analysis of the wear track of the rGO-0.5/epoxy composites with different filler contents

| No. | Content (wt%) | Wear volume ($mm^3$) | Wear rate ($mm^3\ N^{-1}\ m^{-1}$) |
|---|---|---|---|
| 1 | 0 | $(16.4 \pm 0.12) \times 10^{-3}$ | $(9.11 \pm 0.07) \times 10^{-6}$ |
| 2 | 0.1 | $(12.6 \pm 0.18) \times 10^{-3}$ | $(7.00 \pm 0.10) \times 10^{-6}$ |
| 3 | 0.2 | $(1.3 \pm 0.10) \times 10^{-3}$ | $(0.71 \pm 0.05) \times 10^{-6}$ |
| 4 | 0.3 | $(1.4 \pm 0.17) \times 10^{-3}$ | $(0.80 \pm 0.10) \times 10^{-6}$ |
| 5 | 0.4 | $(3.2 \pm 0.19) \times 10^{-3}$ | $(1.80 \pm 0.10) \times 10^{-6}$ |

Table 8 The mechanical properties of the rGO-0.5/epoxy composites with different filler contents

| No. | Content | Modulus (GPa) | Strength (MPa) | Elongation (%) |
|---|---|---|---|---|
| 1 | 0 | $2.55 \pm 0.17$ | $65.2 \pm 1.8$ | $1.0 \pm 0.3$ |
| 2 | 0.1 | $3.02 \pm 0.15$ | $70.6 \pm 1.7$ | $2.1 \pm 0.4$ |
| 3 | 0.2 | $3.20 \pm 0.10$ | $74.2 \pm 2.1$ | $3.4 \pm 0.2$ |
| 4 | 0.3 | $3.11 \pm 0.18$ | $71.8 \pm 2.2$ | $2.6 \pm 0.3$ |
| 5 | 0.4 | $2.89 \pm 0.14$ | $69.5 \pm 1.8$ | $1.1 \pm 0.3$ |

filler both exhibited severe fatigue wear, as shown in Fig. 13. The mechanical properties of the nanocomposites with different filler contents are also listed in Table 8. The data implies that the wear resistance property is closely associated with the toughness of the epoxy composite. This is due to the fact that the enhanced mechanism of both the wear resistance property and toughness of the epoxy-based nanocomposites are dependent on the distribution of nanoparticles and their interface interaction.

## 4. Conclusion

The relationship among tribological performance, physical properties and structure/content of graphene was investigated for graphene-incorporated epoxy composites. The tribological results suggested that GO modified under milder conditions exhibited the optimal performance, where the friction coefficient decreased by 57.9% and the wear rate was reduced by 92.2%. Meanwhile, the rGO-0.5 composite exhibited outstanding physical properties, including enhanced hardness and toughness. The excellent tribological performance and physical properties of the rGO-0.5 composite originated from the structure and morphology of its nanoplatelets. Firstly, the introduced organic chains and reduced nanosheet size contributed to the good dispersion of the nanosheets in epoxy. In addition, the recovery of the intrinsic structure of graphene due to the reduction reaction improved its heat conduction and resistance, which are beneficial for its performance in bearing processing heat and friction heat. Meanwhile, the amino chains and remaining oxygenic groups interacted well with the epoxy system, resulting in strong interfacial interaction. The optimal content of rGO-0.5 in the composite was further studied. It demonstrated that the tribological properties of epoxy could be enhanced significantly by rGO-0.5 with a relatively low content (0.2 wt%), which provides a route for the application of graphene-related nanoparticles in field of tribology.

## Conflicts of interest

There are no conflicts to declare.

## References

1 Y. F. Guo, W. L. Guo and C. F. Chen, Modifying atomic-scale friction between two graphene sheets: A molecular-force-field study, *Phys. Rev. B: Condens. Matter Mater. Phys.*, 2007, **76**, 155429.
2 H. Lee, N. Lee, Y. Seo, *et al.*, Comparison of frictional forces on graphene and graphite, *Nanotechnology*, 2009, **20**(32), 325701.
3 C. G. Lee, Q. Y. Li, K. William, *et al.*, Frictional characteristics of atomically thin sheet, *Science*, 2010, **328**, 76–80.
4 J. Lin, L. Wang and G. Chen, Modification of Graphene Platelets and their Tribological Properties as a Lubricant Additive, *Tribol. Lett.*, 2011, **41**(1), 209–215.
5 D. Berman, A. Erdemir and A. V. Sumant, Few layer graphene to reduce wear and friction on sliding steel surfaces, *Carbon*, 2013, **54**(54), 454–459.
6 J. Ou, J. Wang, S. Liu, *et al.*, Tribology study of reduced graphene oxide sheets on silicon substrate synthesized via covalent assembly, *Langmuir*, 2010, **26**(20), 15830–15836.
7 Y. Li, S. Wang and Q. Wang, Enhancement of tribological properties of polymer composites reinforced by functionalized graphene, *Composites, Part B*, 2017, **120**, 83–91.
8 H. J. Song and N. Li, Frictional behavior of oxide graphene nanosheets as water-base lubricant additive, *Appl. Phys. A: Mater. Sci. Process.*, 2011, **105**(4), 827–832.
9 S. L. Qiu, C. S. Wang, Y. T. Wang, *et al.*, Effects of graphene oxides on the cure behaviors of a tetra functional epoxy resin, *eXPRESS Polym. Lett.*, 2011, **5**(9), 809–818.
10 J. Wu and D. D. L. Chung, Calorimetric study of the effect of carbon fillers on the curing of epoxy, *Carbon*, 2004, **42**(14), 3039–3042.
11 H. Wang, N. Li, Z. W. Xu, *et al.*, Enhanced sheet-sheet welding and interfacial wettability of 3D graphene networks as radiation protection in gamma-irradiated epoxy composites, *Compos. Sci. Technol.*, 2018, **157**(MAR.22), 57–66.
12 I. Zaman, T. T. Phan, H. C. Kuan, *et al.*, Epoxy/graphene platelets nanocomposites with two levels of interface strength, *Polymer*, 2011, **52**(7), 1603–1611.
13 J. A. King, D. R. Klimek, I. Miskioglu, *et al.*, Mechanical properties of graphene nanoplatelet/epoxy composites, *J. Appl. Polym. Sci.*, 2013, **128**(6), 4217–4223.
14 H. Ahmad, M. Fan and D. Hui, Graphene oxide incorporated functional materials: A review, *Composites, Part B*, 2018, **145**, 270–280.
15 Y. Li, Q. Wang, T. Wang, *et al.*, Preparation and tribological properties of graphene oxide/nitrile rubber nanocomposites, *J. Mater. Sci.*, 2012, **47**(2), 730–738.

16 B. Pan, S. Zhang, W. Li, *et al.*, Tribological and mechanical investigation of MC nylon reinforced by modified graphene oxide, *Wear*, 2012, **294–295**(31), 395–401.
17 H. Liu, Y. Li, T. Wang, *et al.*, In situ synthesis and thermal, tribological properties of thermosetting polyimide/graphene oxide nanocomposites, *J. Mater. Sci.*, 2012, **47**(4), 1867–1874.
18 Z. Tai, Y. Chen, Y. An, *et al.*, Tribological Behavior of UHMWPE Reinforced with Graphene Oxide Nanosheets, *Tribol. Lett.*, 2012, **46**(1), 55–63.
19 H. J. Song, N. Li, Y. Li, *et al.*, Preparation and tribological properties of graphene/poly (ether ether ketone) nanocomposites, *J. Mater. Sci.*, 2012, **47**(17), 6436–6443.
20 X. J. Shen, X. Q. Pei, S. Y. Fu, *et al.*, Significantly modified tribological performance of epoxy nanocomposites at very low graphene oxide content, *Polymer*, 2013, **54**(3), 1234–1242.
21 X. J. Shen, X. Q. Pei, Y. Liu, *et al.*, Tribological performance of carbon nanotube–graphene oxide hybrid/epoxy composites, *Composites, Part B*, 2014, **57**(3), 120–125.
22 C. Chen, S. Qiu, M. Cui, *et al.*, Achieving high performance corrosion and wear resistant epoxy coatings via incorporation of noncovalent functionalized graphene, *Carbon*, 2017, **114**, 356–366.
23 F. Lin, Y. Xiang and H. S. Shen, Temperature dependent mechanical properties of graphene reinforced polymer nanocomposites-A molecular dynamics simulation, *Composites, Part B*, 2017, **111**, 261–269.
24 D. Galpaya, M. Wang, G. George, *et al.*, Preparation of graphene oxide/epoxy nanocomposites with significantly improved mechanical properties, *J. Appl. Phys.*, 2014, **116**(5), 031011.
25 W. Li, T. Shang, W. Yang, *et al.*, Effectively Exerting the Reinforcement of Dopamine Reduced Graphene Oxide on Epoxy-Based Composites via Strengthened Interfacial Bonding, *ACS Appl. Mater. Interfaces*, 2016, **8**(20), 13037.
26 Y. J. Wan, L. Cheng, *et al.*, Grafting of epoxy chains onto graphene oxide for epoxy composites with improved mechanical and thermal properties, *Carbon*, 2014, **64**, 467–480.
27 M. Naebe, J. Wang, A. Amini, *et al.*, Mechanical property and structure of covalent functionalized graphene/epoxy nanocomposites, *Sci. Rep.*, 2014, **4**(3), 4375.
28 Y. J. Wan, L. X. Gong, L. C. Tang, *et al.*, Mechanical properties of epoxy composites filled with silane-functionalized graphene oxide, *Composites, Part A*, 2014, **64**(64), 79–89.
29 H. Deng, F. Wu, L. Chen and Z. W. Xu, Enhanced Interfacial Interaction of Epoxy Nanocomposites with Activated Graphene Nanosheets, *J. Appl. Polym. Sci.*, 2014, **131**(23), 41164–41172.
30 W. Li, X. Z. Tang and H. B. Zhang, Simultaneous surface functionalization and reduction of graphene oxide with octadecylamine for electrically conductive polystyrene composites, *Carbon*, 2011, **49**, 4724–4730.
31 A. B. Bourlinos, D. Gournis, D. Petridis, T. Szabo, A. Szeri and I. Dekany, Graphite oxide: chemical reduction to graphite and surface modification with primary aliphatic amines and amino acids, *Langmuir*, 2003, **19**, 6050–6055.
32 Y. W. Cao, J. C. Feng and P. Y. Wu, Alkyl–functionalized graphene nanosheets with improved lipophilicity, *Carbon*, 2010, **48**, 1683–1685.
33 G. Wang, X. Shen, B. Wang, J. Yao and J. Park, Synthesis and characterization of hydrophilic and organophilic graphene nanosheets, *Carbon*, 2009, **47**, 1359–1364.
34 Z. Y. Lin, Y. Liu and C. P. Wong, Facile fabrication of superhydrophobic octadecylamine–functionalized graphite oxide film, *Langmuir*, 2010, **26**, 16110–16114.
35 T. J. Bao, Z. Y. Wang, Y. Zhao, *et al.*, Composition, Structure and Morphology Evolution of Octadecylamine (ODA)–Reduced Graphene Oxide and Its Dispersion Stability under Different Reaction Conditions, *Materials*, 2018, **11**(9), 1710–1724.
36 Y. Zhao, H. Ding and Q. Zhong, Preparation and characterization of aminated graphite oxide for CO2 capture, *Appl. Surf. Sci.*, 2012, **258**(10), 4301–4307.
37 J. Shen, W. Huang, L. Wu, *et al.*, Study on amino-functionalized multiwalled carbon nanotubes, *Mater. Sci. Eng., A*, 2007, **464**(1–2), 151–156.
38 S. Stankovich, D. A. Dikin, G. H. B. Dommett, K. M. Kohlhaas, E. J. Zimney, E. A. Stach, R. D. Piner, S. T. Nguyen and R. S. Ruoff, Graphene-based composite materials, *Nature*, 2006, **442**, 282.
39 M. Hirata, T. Gotou, S. Horiuchi, M. Fujiwara and M. Ohba, Thin–film particles of graphite oxide 1: high–yield synthesis and flexibility of the particles, *Carbon*, 2004, **42**, 2929–2937.
40 T. N. Zhou, F. Chen, K. Liu, H. Deng, Q. Zhang, J. W. Feng, *et al.*, A simple and efficient method to prepare graphene by reduction of graphite oxide with sodium hydrosulfite, *Nanotechnology*, 2011, **22**, 045704.
41 G. Tang, Z. G. Jiang, X. Li, *et al.*, Electrically conductive rubbery epoxy/diamine-functionalized graphene nanocomposites with improved mechanical properties, *Composites, Part B*, 2014, **67**, 564–570.
42 M. Nonahal, M. R. Saeb, S. Hassan Jafari, *et al.*, Design, preparation, and characterization of fast cure epoxy/amine-functionalized graphene oxide nanocomposites, *Polym. Compos.*, 2017, **39**(S4), 2016–2027.
43 S. Stankovich, D. A. Dikin, R. D. Piner, *et al.*, Synthesis of graphene-based nanosheets via chemical reduction of exfoliated graphite oxide, *Carbon*, 2007, **45**(7), 1558–1565.
44 H. J. Kim, K. J. Seo and D. E. Kim, Investigation of mechanical behaviour of single- and multi-layer graphene by using molecular dynamics simulation, *Int. J. Precis. Eng. Manuf.*, 2016, **17**, 1693–1701.
45 N. K. Myshkin, M. I. Petrokovets and A. V. Kovalev, Tribology of polymers: Adhesion, friction, wear, and mass-transfer, *Tribol. Int.*, 2005, **38**(11), 910–921.
46 S. Xia, Y. Liu, F. Pei, *et al.*, Identical steady tribological performance of graphene-oxide-strengthened polyurethane/epoxy interpenetrating polymer networks derived from graphene nanosheet, *Polymer*, 2015, **64**, 62–68.
47 S. Z. Wen. *Principles of Tribology*, Tsinghua University Press, Beijing, 2nd edn, 2002, pp. 277–278.

 

48 C. Bao, Y. Guo, L. Song, *et al.*, In situ preparation of functionalized graphene oxide/epoxy nanocomposites with effective reinforcements, *J. Mater. Chem.*, 2011, **21**(35), 13290–13298.

49 M. Fang, K. Wang, H. Lu, *et al.*, Single-layer graphene nanosheets with controlled grafting of polymer chains, *J. Mater. Chem.*, 2010, **20**(10), 1982–1992.

50 E. Sancaktar and D. Aussawasathien, Nanocomposites of Epoxy with Electrospun Carbon Nanofibers: Mechanical Behavior, *J. Adhes.*, 2009, **85**(4–5), 160–179.

51 B. B. Johnsen, A. J. Kinloch, R. D. Mohammed, *et al.*, Toughening mechanisms of nanoparticle-modified epoxy polymers, *Polymer*, 2007, **48**(2), 530–541.

52 W. S. Kang, K. Y. Rhee and S. J. Park, Influence of surface energetics of graphene oxide on fracture toughness of epoxy nanocomposites, *Composites, Part B*, 2017, **114**, 175–183.

53 T. Ramanathan, A. A. Abdala, S. Stankovich, *et al.*, Functionalized graphene sheets for polymer nanocomposites, *Nat. Nanotechnol.*, 2008, **3**(6), 327–331.